CHEMISTRY OF MATERIALS

ARTICLE

pubs.acs.org/cm

Ab Initio Molecular Dynamics Simulations of the Cooperative Adsorption of Hydrazine and Water on Copper Surfaces: Implications for Shape Control of Nanoparticles

Thomas D. Daff*,†,‡ and Nora H. de Leeuw*,‡

†School of Crystallography, Birkbeck College, Malet Street, London WC1E 7HX, United Kingdom

‡Department of Chemistry, University College London, 20 Gordon Street, London, WC1H 0AJ, United Kingdom

ABSTRACT: We have used density functional theory and ab initio molecular dynamics simulations to pursue an accurate description of the hydrazine−water system adsorbed on low-index surfaces of copper. Experimental evidence suggests that shape control in the reverse micelle synthesis of nanoparticles may be affected by differences in interactions of the reducing agent (hydrazine) with the surfaces. First, we have modeled the competitive adsorption of single molecules of water and hydrazine from the gas phase, which, however, shows no preference for selective adsorption. Subsequent molecular dynamics simulations of a system of hydrazine cooperatively adsorbed with a hydration shell reveals a strong influence on the adsorption behavior from the network of hydrogen bonding. A comparison of the thermodynamics of simulations with and without hydrazine adsorbed at the surface suggests that hydrazine will adsorb on the (111) surface but not on the (100) surface. These findings explain the experimental crystal shapes induced by reducing agent through a mechanism of binding to and accelerating the growth of the (111) faces.

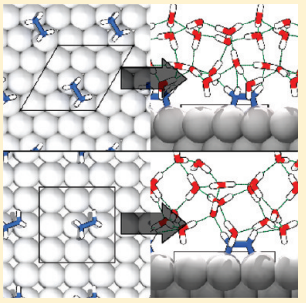

KEYWORDS: surface and interfacial phenomena, theory and modeling, molecular crystals

INTRODUCTION

The size, shape, and structural control of nanoparticle growth is an important issue in the design of materials with novel, fine-tuned properties.[1−5] Experimental work has developed a number of viable methods for the production of nanoparticles, but much of the design of these processes is based on empirical observations.[6−11] The method of copper particle synthesis from reverse micelles is a chemical reduction process that uses hydrazine to reduce a copper salt in water-in-oil droplets.[12−14] Many factors affect the resultant particle morphology by altering the reaction conditions: for example, the composition of the water−oil mixture.[15] In this work we have focused on the shape control obtained as an effect of the concentration of the reducing agent.[16,17]

Two types of copper particle formed in the synthesis are cuboctahedral- and decahedral-based shapes as shown in Figure 1. The cuboctahedra cover the range of shapes from cubic particles, containing only the (100) copper surface, to octahedra, which have only (111) surfaces. The intermediate shapes exist with varying proportions of the two surfaces. An increase in the hydrazine concentration results in the distribution of shapes produced shifting toward more cubic particles. The decahedral particles have a 5-fold rotational axis where five tetrahedra are joined, giving (111) surface faces. Increasing the hydrazine concentration results in elongation along the rotational axis, giving a truncated decahedron and exposing (100) surface on the sides. Interaction of the reaction mixture with the different surfaces is important in determining the final morphologies. Therefore, in this work we have compared the interactions of hydrazine and water on the close-packed, and most stable, (111) surface with the square-packed (100) surface that is seen in the experimental particles and, as a less stable surface,[18] is potentially more reactive.

We aim to improve nanoparticle production methods by gaining an understanding of the processes occurring at the molecular level. Initial attempts to rationalize experimental observations have compared isolated gas-phase adsorption of the reducing agent on different copper surfaces.[19] Although the conclusions drawn align with the experimental data, a number of approximations were necessarily made in the model. In this work we have extended those calculations by providing a much better model of the experimental conditions. In particular we have looked at the effect of water as an important component of the reaction system.

We use ab initio methods to model the systems of copper surfaces, hydrazine, and water. We first consider the complete displacement of water from the copper surfaces to adsorb the hydrazine. This method of competitive adsorption has been used successfully for other molecules,[20] but the results in our case are inconclusive and highlight the need to consider the complete system of hydrazine and water cooperatively adsorbed at the copper surfaces. As a precursor to this combined study, we first use molecular crystal structures to gauge the suitability of the density functional theory (DFT) method for the simulation of a mixed system of hydrazine and water. Finally we run a number of ab initio molecular dynamics (MD) simulations of the cooperative adsorption of both species to compare the thermodynamics

Received: November 3, 2010
Revised: April 5, 2011
Published: May 05, 2011

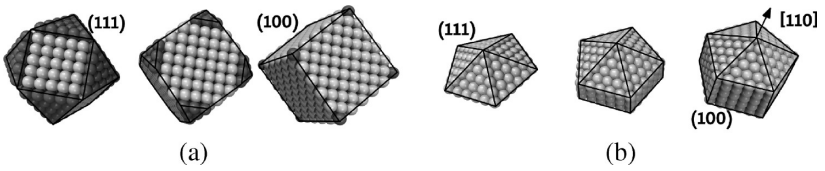

Figure 1. Schematic of shapes of copper particles produced in experimental synthesis, with spheres showing atomic positions and outlines showing general particle shapes: (a) cuboctahedron with growth on (111) faces to give a cubic particle; (b) truncated decahedron with growth along the [110] direction, elongating the particle.

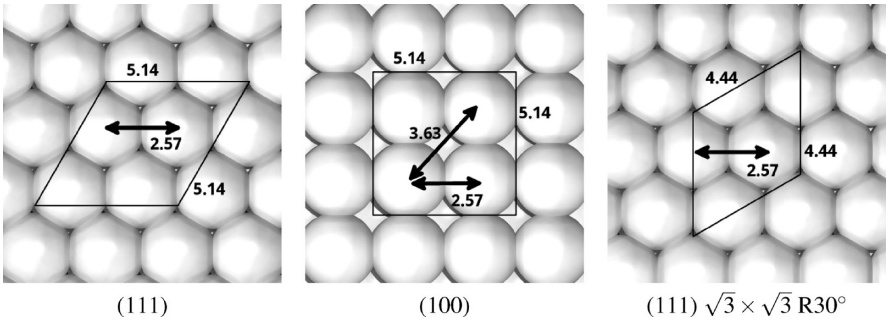

Figure 2. Plan views of the copper surface structures showing the 2 × 2 simulation cells used for isolated adsorption and the $\sqrt{3} \times \sqrt{3}$ R30° cell also used for the (111) surface (distances are given in angstroms).

during simulation and study the extensive hydrogen-bonded structures that form through snapshots at various points. Similar methods have been used to study successfully both water alone and water adsorbed at copper surfaces.[21,22] Modeling of surface adsorption processes of molecules with explicit water has previously been limited to classical parametrizations and multiscale models[23,24] although more recently ab initio simulations have become viable.[25] The work presented here is a fully ab initio treatment of several models up to cooperative adsorption across different surfaces.

METHODS

All our calculations have been carried out at the DFT level of theory using plane-wave pseudopotential methods implemented in the Vienna ab initio simulation package (VASP).[26−29] The details of the calculations are identical to those given in ref 19. The total energy calculations employed the generalized gradient approximation (GGA) PW91 projector augmented wave (PAW) potentials[30−33] with a plane-wave cutoff energy converged at 400 eV. Self-consistent electronic minimization was converged to 0.1 meV between consecutive steps. The surfaces are modeled as periodic slabs cut from the optimized bulk metal with six atomic layers, the bottom two of which are fixed at their bulk positions. The slabs, including all the adsorbates, are separated by a vacuum gap of at least 10 Å perpendicular to the surface. For the 2 × 2 slab we have used a 5 × 5 × 1 *k*-point grid, whereas for the larger cells we have used a reduced 3 × 3 × 1 grid. The structures of the surfaces are shown in Figure 2.

The surface structures were optimized with the conjugate gradient minimizer in VASP. The ions are moved toward the ground-state structure according to the forces, improving on previous iterations by refining steps to reduce the parallel components in the forces in successive steps. The convergence criterion was set at 0.1 meV in the total energy between successive ionic steps.

The dynamics of the systems were investigated with Born−Oppenheimer molecular dynamics (BOMD), also by use of VASP. The forces at each time step are calculated from the ground-state

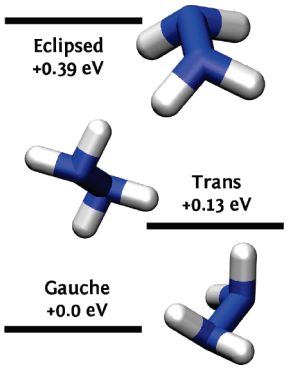

Figure 3. Stability of conformers of hydrazine with their calculated energies relative to the most stable gauche conformer.

electronic structure and the positions and velocities of the ions integrated according to Newtonian mechanics. The models were equilibrated at the desired temperature with velocity scaling. During data collection runs, the temperature is controlled with a Nosé thermostat. The overall accuracy of the calculations was lowered from the total energy calculations to save computational costs, but we ensured that the forces were well converged at each step so that the energy remained stable by using time steps up to 1 fs. The relative energy drift per atom in all cases was about -5×10^{-8} ps^{-1}.

The adsorption energies of individual molecules and of the complete hydrazine−water system are calculated as the difference between the calculated total energy of the surface−adsorbate systems and the sum of the energies of an identical isolated relaxed surface and all the isolated individual molecules in the system, where the ideal geometry for the hydrazine is the relaxed gauche conformer, shown in Figure 3. All energies are given per simulation cell, as we consider only a single hydrazine molecule in each cell.

The images of the simulated systems in this work show the bonding in the molecules and their intermolecular interactions, where bonding is assigned by a distance cutoff. Hydrogen bonding is calculated by

dx.doi.org/10.1021/cm103164w |*Chem. Mater.* 2011, 23, 2718–2728

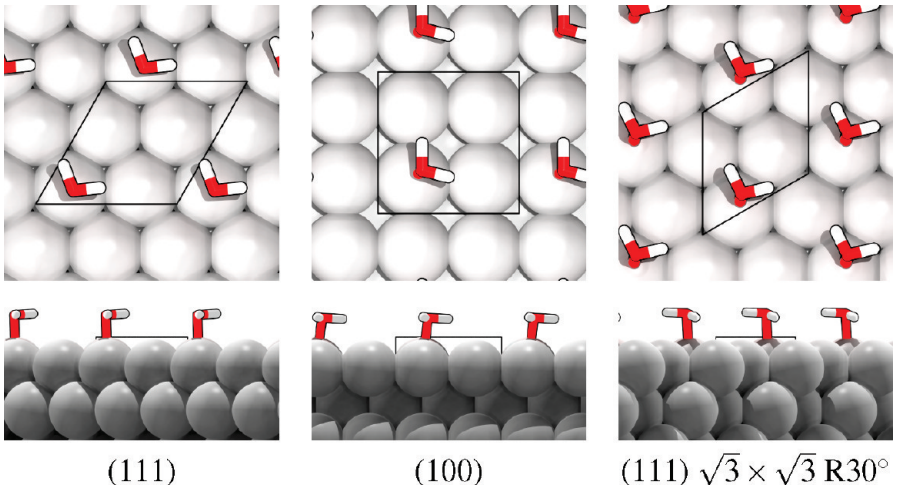

Figure 4. Optimum geometries for a single water molecule adsorbed on the low-index copper surfaces showing the simulation cell and periodic images as plan (top) and side (bottom) views (O = red, H = white).

Table 1. Adsorption Energies for Hydrazine and Water Molecules and the Energy Difference for Displacing One and Two Water Molecules with a Hydrazine Molecule

surface	cell	E_{ads,H_2O}/ eV	E_{ads,N_2H_4}/ eV	$\Delta E_{H_2O \rightarrow N_2H_4}$/ eV	$\Delta E_{2H_2O \rightarrow N_2H_4}$/ eV
(111)	2 × 2	−0.17	−0.42	−0.25	−0.08
(100)	2 × 2	−0.24	−0.57	−0.34	−0.10
(111)	$\sqrt{3} \times \sqrt{3}$ R30°	−0.21	−0.32	−0.12	0.09

considering a distance cutoff of 2.5 Å and excluding the bonded hydrogen atoms at distances less than 1.2 Å. As the structures are reasonably ordered, this protocol produced an acceptable distribution without having to consider other factors, such as the bonding angles.[34]

■ ISOLATED COMPETITIVE SURFACE ADSORPTION

As a first approximation to the adsorption of hydrazine in the presence of water, the relative strengths of adsorption of the two molecules can be compared directly to give an estimate of the energy required to displace one molecule with the other. Although the adsorption behavior of water at copper surfaces has been studied previously, we reconsider it here as the uniform treatment of both the hydrazine and water adsorption by the same methods and identical systems allows for a direct quantitative comparison.

A single water molecule has been adsorbed in the 2 × 2 simulation cell at each of the copper surfaces, and the optimized geometry has been calculated. The ideal geometry for the adsorption of a water molecule is found to match the expected result for each surface.[35−39] Although the water molecule has fewer degrees of freedom than hydrazine (e.g., torsional angles), the potential energy surface (PES) of adsorption for the water has a number of local minima and is quite flat near the global minimum.[36] The correlation of our optimized structures with previous studies indicates that they have relaxed to the global minima and not local minima. The molecule binds through the oxygen atom in an atop position on a surface copper atom, with the molecule lying nearly flat with respect to the surface, although slight variations occur in the geometries on the different surfaces.

The adsorption structures are shown in Figure 4. On the (111) surface, the hydrogen atoms are pointing up slightly from the plane of the surface. On the (100) surface, which has a lower packing density than the (111) surface, there is a slight descent of the hydrogen atoms into the hollows between the copper atoms. The orientation of the molecule on the (111) $\sqrt{3} \times \sqrt{3}$ R30° surface is slightly more skewed, but the figure also shows that the separation between the periodic images of the molecule is smaller in this higher surface coverage, which may lead to spurious interactions that affect the adsorption.

The adsorption energies for each surface/water system are given in Table 1. The strongest adsorption energy for hydrazine under identical conditions to the present calculations, taken from ref 19, are used to calculate the energy of displacement. The adsorption strength of water to each surface follows a similar trend to the adsorption of hydrazine, with the adsorption energy more exothermic on the less stable surface. Binding of both hydrazine and water is stronger on the (100) surface than on the most stable (111) surface. The magnitudes of the values correlate well with previous data.[35,36]

Considering, in the first instance, a direct displacement of one water molecule by hydrazine, the difference in adsorption energies is exothermic in all cases, which implies that the hydrazine adsorption is preferred for single-molecule exchange. The order of the binding strength of hydrazine to the different surfaces does not change with the additional consideration of water; binding with displacement of water is still stronger on the (100) surface than on the (111) surface.

As the hydrazine molecule is effectively double the size of individual water molecules, at high coverage it would probably displace two or more water molecules from the surface. Considering the difference in adsorption energies between hydrazine and two water molecules brings the displacement energies for both the surfaces with a 2 × 2 cell closer together and closer to zero; adsorption is only slightly exothermic when two water molecules are replaced with hydrazine. Hydrazine is still slightly favored over water, although the margin is much smaller and the difference between adsorption on the different surfaces is negligible.

As we have noted in previous adsorption studies, this gas-phase approach fails to account for many important factors.

dx.doi.org/10.1021/cm103164w |*Chem. Mater.* 2011, 23, 2718–2728

Table 2. Structural Parameters of Crystalline Hydrazine with Molecules in Eclipsed and Gauche Conformations[a]

	ref 43	eclipsed	gauche
		Unit Cell Parameters	
a/Å	3.56	3.31 (−7.0%)	3.29 (−7.5%)
b/Å	5.78	5.37 (−7.2%)	5.40 (−6.6%)
c/Å	4.53	4.53 (−6.3%)	4.46 (−1.5%)
β/deg	109.5	106.3 (−3.0%)	109.8 (0.3%)
V/Å^3	87.9	72.3 (−17.7%)	74.7 (−15.0%)
ρ/g·cm^{-3}	1.21	1.47 (7.2%[b])	1.42 (3.8%[b])
		Fractional Atomic Coordinates	
Nx_1	0.037	0.025	0.022
Ny_1	0	−0.014	−0.000
Nz_1	0.362	0.378	0.359
Nx_2	0.736	0.744	0.736
Ny_2	0	0.012	0.001
Nz_2	0.050	0.047	0.032
		Atomic Separations	
d_{N-N}/Å	1.46	1.46 (−0.2%)	1.45 (−1.0%)
N_2-N_3/Å	3.19	2.90 (−9.2%)	3.00 (−5.9%)
N_2-N_8/Å	3.25	3.08 (−5.1%)	3.16 (−2.7%)
N_5-N_4/Å	3.30	3.10 (−6.1%)	3.08 (−6.7%)
N_7-N_5/Å	3.62	3.23 (−10.8%)	3.44 (−5.1%)
N_5-N_6/Å	3.67	3.33 (−9.3%)	3.45 (−6.1%)
		Three-Body Angles	
$N_2N_3N_2$/deg	125	136 (8.5%)	128 (2.5%)
$N_5N_4N_5$/deg	122	112 (−1.7%)	123 (0.4%)
$N_2N_3N_4$/deg	114	110 (−3.2%)	109 (−4.7%)
$N_3N_4N_5$/deg	131	102 (−22.0%)	103 (−21.4%)
$N_1N_2N_8$/deg	90	86 (−4.9%)	82 (−8.6%)
		Binding Energy	
E_{bind}/kJ·mol^{-1}		−23.5	−45.0

[a] Unit cell parameters, fractional atomic coordinates, atomic separations, three-body angles, and binding energy are given for each structure with the percentage difference from the X-ray crystallographic structure. [b] Density comparisons are taken against the experimental density extrapolated to 1.37 g·cm^{-3} at 0 K.

A transfer of molecules to and from an isolated gas phase is unrealistic for the system that we are interested in, as is considering an isolated molecule on the relevant surfaces, particularly as our attempt to isolate the adsorbed molecules has ignored the strong structure-influencing properties of intermolecular interactions, which is exemplified to some extent by the $\sqrt{3} \times \sqrt{3}$ R30° (111) surface.

Although the adsorption displacing two isolated water molecules is exothermic for both the 2 × 2 surface cells, the $\sqrt{3} \times \sqrt{3}$ R30° cell for the (111) surface is an exception. Here the adsorption energy per water molecule is more than half that for hydrazine, due to the effect of intermolecular interactions, as indicated by the difference in adsorption energies for the two cell sizes of this surface. A decrease in the cell size—and increase in water coverage—increases the adsorption strength of water at the surface. Water undergoes cooperative adsorption; the exposed $\delta-$ on the oxygen atom and $\delta+$ on the polarized hydrogen atoms of the periodic images will have an attractive interaction. In the $\sqrt{3} \times \sqrt{3}$ R30° cell, the separation of periodic oxygen atoms is 4.45 Å and the closest hydrogen to a periodic oxygen is 3.53 Å. In the 2 × 2 cell, these distances have increased to 5.14 and 4.16 Å, respectively, diminishing the interaction and resulting in overall weaker adsorption. In this study the water is interacting with its own periodic images, but the cooperative effect of hydrogen-bonded ring structures of many molecules has been found to greatly stabilize the adsorption of water on various metal surfaces.[40,41]

In contrast to the adsorption of water, the decrease in the size of the (111) simulation cell enhances repulsive, destabilizing interactions between the hydrazine periodic images more than any cooperative, stabilizing interactions in this particular geometry (Table 1). Hence, adsorption of hydrazine in the smaller cell is overall weaker. The smaller cell size is closer to the limit of monolayer hydrazine coverage, and unlike the oxygen in water, the nitrogen atoms in the hydrazine are much less exposed and are obscured from the periodic images by the hydrogen atoms, which will interact repulsively. Combined with the opposite change in the adsorption strength of water, in the smaller (111) $\sqrt{3} \times \sqrt{3}$ R30° surface cell the adsorption of hydrazine is not sufficiently strong to displace the equivalent of two water molecules on thermodynamic grounds. Even when the case of the more isolated hydrazine in the 2 × 2 cell is considered, displacing two water molecules at the higher coverage still yields 0 eV for adsorption. However, in the experimental systems the hydrazine is in a dilute solution and the large separation expected between adsorbed molecules will effectively remove hydrazine−hydrazine interactions. The intermolecular interactions between molecules at the surface will be replaced by the hydration shell of the molecule, and the interactions between the hydrazine and water, as well as with the surface, will be key in stabilizing the adsorption.

Clearly this method of comparison of displacing isolated adsorbates is unsuitable for the investigation of the copper−hydrazine−water system, although it has identified areas for improvement. In particular, consideration of water in this way has so far not demonstrated any major effect on the relative binding interactions to differentiate the experimentally observed adsorption behavior of hydrazine on the different copper surfaces. To gain a reasonable understanding of the copper system, the cooperative adsorption and behavior of the two species needs to be studied.

HYDRAZINE CRYSTAL STRUCTURE

The cooperative adsorption of water and hydrazine will involve the interactions of both species, not only with the surface but also with each other. As it is our aim to account for the effects from intermolecular interactions in our calculations, it is useful to study first the molecular crystal structures of the adsorbing species and hence the individual interactions between the molecules, which will provide a measure of the accuracy with which the method describes these interactions. Although pure water has been very well studied previously as both solid and liquid by these DFT methods,[41,42] only crystallographic data exist for the hydrazine and hydrazine monohydrate molecular crystals.

X-ray studies have provided the positions of the nitrogen atoms in the crystalline structure of hydrazine,[43] from which the authors have deduced the least stable eclipsed conformer for the molecule in the structure, with the hydrogen atoms satisfying

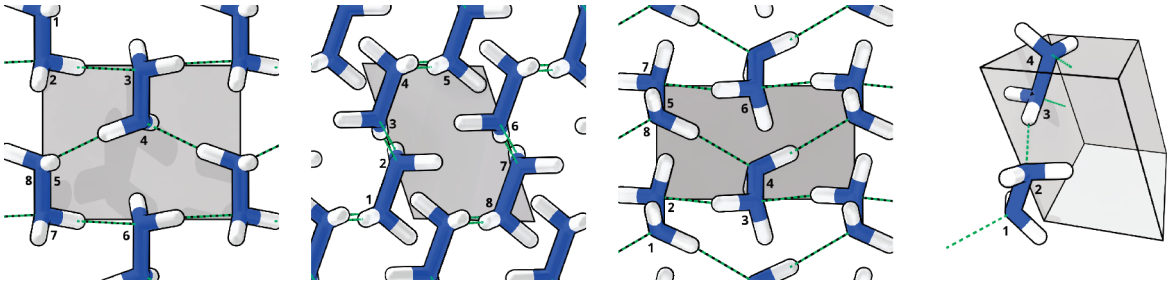

Figure 5. Crystal structure of gauche molecular hydrazine viewed (left to right) along the [100], [010], and [001] directions and a single formula unit in the unit cell (N = blue, H = white; N atoms were indexed according to Table 2).

C_{2h}^2—$P2_1/m$ crystal symmetry. However, subsequent nuclear magnetic resonance (NMR) work has concluded that the molecule is staggered with overall C_2^2—$P2_1$ crystal symmetry.[44] Here we have modeled both structures for comparison.

The optimized geometry has been calculated for the two-molecule unit cell, and relevant structural data are given in Table 2. The nitrogen atoms in Table 2 are indexed and the structure for the crystal with gauche molecules is shown in Figure 5. The enthalpy of crystal formation favors this staggered structure over an eclipsed one; the binding energy for the gauche crystal at -45.0 kJ·mol^{-1} is nearly double that of the crystal containing the eclipsed conformer, supporting the findings from NMR for the staggered conformation of the molecule and in contrast to the suggestion by Collin and Lipscomb.[43] The thermodynamic data provided in the X-ray study can also be compared with the calculated values. The heat of vaporization for hydrazine is given as 45 kJ·mol^{-1} (10.7 kcal·mol^{-1}), which is similar to the calculated binding energy for the gauche conformation and much greater than that for the eclipsed conformer. Although the binding energy is not necessarily directly comparable to the enthalpy of vaporization, it gives a reasonable approximation, if we assume a noninteracting gas for the hydrazine. The proportion of the energy attributed to the hydrogen bonding is the major component at 29 kJ·mol^{-1} (7 kcal·mol^{-1}) and is probably well accounted for by the model. The remaining forces due to dispersion interactions are known not to be fully accounted for by the DFT method.[45] However, much of the error has been shown to be recovered when the PW91 functional is used for small, hydrogen-bonded molecules when the accuracy in the interaction energy is estimated to be within around 10%.[46] In any case, discrepancies in the dispersion forces will have only minimal impact on the geometries of the structures that are obtained, as they are reasonably isotropic in comparison to the directional nature of the hydrogen bonding.[47]

Comparison of both structures with the X-ray structure shows a number of significant differences, particularly in the cell lengths and volumes (Table 2). As our calculations are carried out for the ground-state optimized structures at 0 K, contraction will be expected from the crystal structure as measured at finite temperature (~-15 °C). The density for the solid when extrapolated to 0 K gives a much better agreement, although the calculated structures are slightly more dense.[48] The relative positions of the atoms and orientation of the molecules are in moderate agreement. Although the cell size differences are generally anisotropic, the overall structural arrangements are fairly well replicated, particularly in the gauche crystal. The majority of the hydrogen bonds lie close to the *ab* plane with the N—N bonds aligned nearer to the *c* vector. A greater contraction of the hydrogen bonds would account for the larger thermal dependence in *a* and *b* over *c*. Although the atom separations show an almost uniform contraction, both structures fail substantially to reproduce at least one of the angles.

Overall, the method adequately reproduces the hydrogen-bonded structure of the hydrazine crystal. It also confirms that the gauche conformation is the most favored configuration for the molecule in the crystal structure.

HYDRAZINE MONOHYDRATE CRYSTAL STRUCTURE

For the study of the combined behavior of water and hydrazine, the monohydrate crystal that forms at low temperatures provides a structure, shown in Figure 6, that is formed wholly from intermolecular interactions between the two different molecules. Each hydrazine molecule in the structure is hydrogen-bonded to six water molecules, with all four of its hydrogen atoms forming hydrogen bonds with different water molecules. Each water molecule also has six hydrogen bonds, in a nearly octahedral arrangement; the two exposed lone pairs on the oxygen are involved in hydrogen bonds to four hydrazine molecules. The unit cell, containing three hydrazine—water pairs, was optimized to give the ground-state structure.

Comparison of the simulated structure with the one measured by X-ray crystallography[49] is given in Table 3. As the structure was obtained at finite temperature (-165 °C), the volume of the ground-state calculated structure is substantially smaller. The contraction is reasonably isotropic, where the cell has maintained the hexagonal shape, and it is also less than for the pure hydrazine crystal, which was of course obtained at a higher temperature. Aside from the hydrogen-bond distances that have contracted, the structure is reproduced well by the simulation. Most of the angles fall within about 1% of the experimental values, with an even spread of smaller and larger values.

The calculated crystal structures show that the method gives a reasonable description of the hydrazine intermolecular interactions but a much better description of the interactions between hydrazine and water. As the modeled surface—adsorbate systems contain a relatively low concentration of hydrazine, the intermolecular interactions of water itself and with the hydrazine will be the most important in determining the thermodynamic behavior at the surface, and the method is therefore suitable for the present calculations.

COOPERATIVE SURFACE ADSORPTION

The molecular crystal structures have indicated that hydrogen bonding is a major factor in determining both the energetics and geometries of the interactions between hydrazine and water. These will, therefore, also have an important effect in

dx.doi.org/10.1021/cm103164w |*Chem. Mater.* 2011, 23, 2718–2728

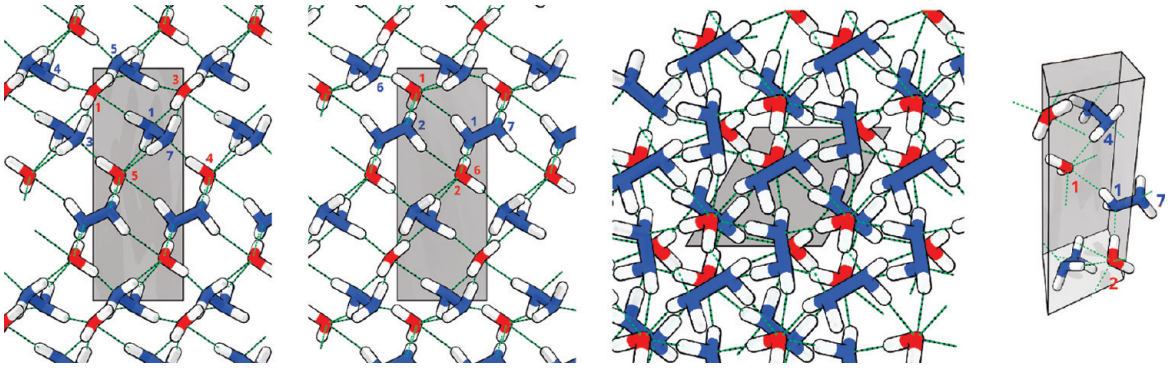

Figure 6. Crystal structure of molecular hydrazine monohydrate viewed (left to right) along the [100], [010], and [001] directions and a single formula unit in the unit cell (N = blue, O = red, H = white; atoms were indexed according to Table 3).

Table 3. Structural Parameters of Crystalline Hydrazine Monohydrate[a]

	ref 49	this work	difference/%
	Unit Cell Structure		
a/Å	4.873	4.711	−3.32
b/Å	4.873	4.711	−3.32
c/Å	10.94	10.49	−4.07
γ/deg	120	120	0
V/Å^3	225.0	201.7	−10.34
	Fractional Atomic Coordinates		
Nx	0.5954	0.5922	
Ny	0.8373	0.8338	
Nz	0.3124	0.3092	
Ox	0.7268	0.7217	
Oy	0	0	
Oz	0.8333	0.8333	
	Atomic Separations		
O_1−N_2/Å	2.790	2.688	−3.66
O_1−N_1/Å	3.113	2.971	−4.56
O_1−N_3/Å	3.149	3.029	−3.81
N_1−N_7/Å	1.447	1.447	0
	Three-Body Angles		
$N_1O_1N_2$/deg	111.2	112.6	1.28
$N_1O_1N_3$/deg	74.2	74.6	0.55
$N_1O_1N_4$/deg	145.9	146.1	0.12
$N_1O_1N_5$/deg	82.6	82.6	−0.02
$N_1O_1N_6$/deg	87.6	86.5	−1.29
$N_2O_1N_3$/deg	78.7	78.8	0.08
$N_2O_1N_5$/deg	161	160.7	−0.16
$N_2O_1N_6$/deg	113.8	112.7	−0.95
$N_3O_1N_5$/deg	93.4	94.9	1.63
$O_2N_1O_6$/deg	107.2	106.4	−0.78
$O_1N_1O_6$/deg	99.7	99.8	0.08
$O_6N_1N_7$/deg	120.8	118.0	−2.29
$O_1N_1O_2$/deg	111.2	112.6	1.28
$O_2N_1N_7$/deg	109.8	110.7	0.85
$O_1N_1N_7$/deg	107.7	108.7	0.91

[a] Unit cell structure, fractional atomic coordinates, atomic separations, and three-body angles are given for each structure with the percentage difference from the X-ray crystallographic structure.

competition with the geometric and positional factors of the interaction with the surfaces already seen for the isolated molecules, and any intermolecular interactions arising from the periodic cell images. As the size of the system increases, the large number of degrees of freedom makes it less feasible to construct and refine expected adsorption geometries to search for low-energy minima or the global minimum on the PES. Hence, with the inclusion of water in the system, we have used MD to explore the entire system and generate a range of cooperative adsorption geometries.

In our MD simulations we have increased the size of the simulation cell to a 3 × 3 supercell, where the hydrazine molecule has been adsorbed together with a shell of 12 water molecules, ensuring a sufficient gap between the periodic images of the slabs. With 54 copper atoms in the surface, the total simulation size is 96 atoms. This setup also isolates the hydrazine from its lateral periodic images and allows space for a hydration shell of the molecule to form.

Although the time scales currently achievable with BOMD will give only limited statistics for sampling of the system, particularly for long time scale processes, with no guarantee that the simulation will sample the ground state, the results will give an indication of the interplay of the important interactions and how the system behaves at finite temperatures. Snapshots taken at low-energy positions throughout the trajectory will isolate the strong interactions that determine the thermodynamic minima.

As the adsorption/desorption processes are unlikely to occur spontaneously during the short simulations, two trajectories were begun on each surface, one with hydrazine adsorbed onto the surface copper atoms and one with the molecule suspended in the water above the surfaces. The initial configurations for the water were obtained from previous simulations that had thermalizd and then displaced slightly to accommodate the addition of hydrazine. Previous studies have suggested that the water is overly structured at 300 K[42] with these methods; hence the systems for the copper surfaces were equilibrated by scaling the velocities at each step to a temperature of 350 K for at least 2 ps before they were run in the constant number, volume, and temperature (NVT) ensemble for between 12 and 15 ps with the thermostat temperature also at 350 K. Geometry optimization to the local ground-state structure was also carried out on snapshots at various instances throughout the simulations.

(111) Surface. A stable minimum on the PES was found for a configuration with hydrazine adsorbed at the surface by bridging surface copper atoms. Very little diffusion occurs around the

dx.doi.org/10.1021/cm103164w |*Chem. Mater.* 2011, 23, 2718–2728

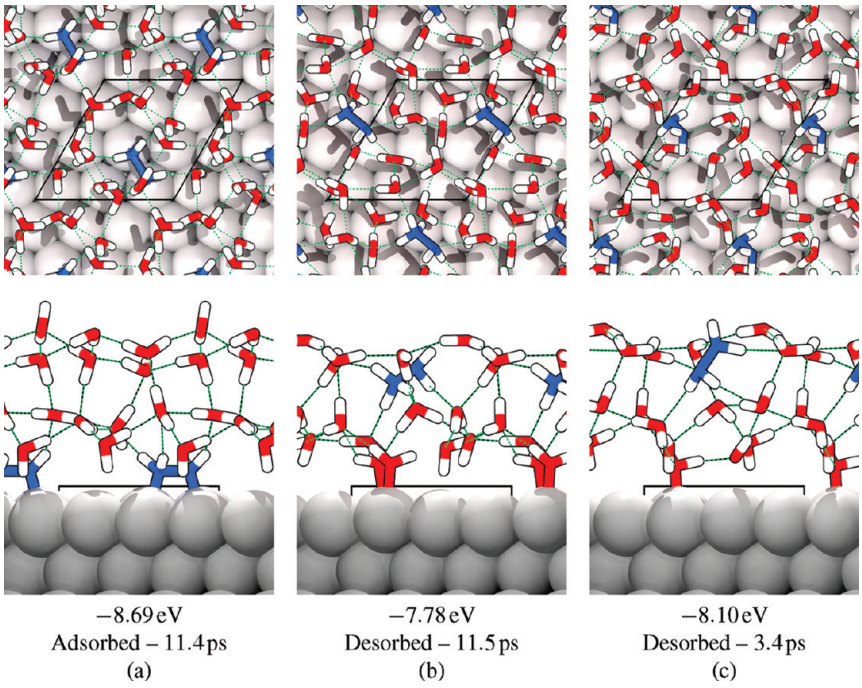

Figure 7. Optimised snapshots at the indicated times after equilibration showing cooperative adsorption of hydrazine and water on the (111) surface (N = blue, O = red, H = white). Energies are the adsorption energy for the ground state optimized structure from the gas phase per simulation cell.

adsorbed species during the simulation, particularly in the latter stages of the simulation, as the snapshots from this phase of the MD simulation all minimize to an identical low-energy structure.

Previous work on the adsorption of hydrazine from the gas phase onto vacuum surfaces has shown that, on the (111) surface, hydrazine thermodynamically prefers adsorption through a single interaction to copper rather than a configuration bridging two surface atoms. In the presence of water, however, the bridging configuration has been stabilized significantly and remains for the duration of the simulation. The bridging configuration is disfavored at the vacuum interface as steric factors prevent the molecule binding close to the surface in the fully relaxed gauche conformation. The energy penalty to torsionally rotate the N−N bond and the resulting longer Cu−N bonds is not outweighed by the benefit of both nitrogen atoms strongly interacting with the surface. However, the energy difference between the optimum bridging configuration and the singly bound gauche adsorption for the isolated molecules is not so large that the gauche bridging conformer could not be stabilized. In the presence of water, however, the bridging hydrazine molecule relaxes to an eclipsed conformation, even in the most favored of the optimized snapshots, although for the isolated molecule the eclipsed conformer is 0.39 eV less stable than the gauche (Figure 3).[19]

A closer look at the geometry of cooperative adsorption (see Figure 7a) shows that stabilization originates from a highly structured network of hydrogen bonds between all the molecules. The hydrazine molecule itself is involved in four hydrogen bonds to the surrounding water, and the energy benefit of the hydrogen bonding will easily outweigh the torsional energy penalty. As a result of the periodic boundaries of the simulation cell, the water is also involved in a longer-range network of hydrogen bonds. The distance between periodic hydrazine molecules is suitable for the formation of a chain of hydrogen bonds, with chains of two water molecules connecting the periodic images of the hydrazine molecules. The different orientations of the hydrogen-bonded chains ultimately result in ring structures close to the surface. The water molecules are oriented only with hydrogen atoms facing the surface at a distance of about 2.3 Å; there is no direct adsorption through Cu−O bonding.

The lower layer of molecules near the surface is also hydrogen-bonded to an upper layer of water molecules that are in a stable network of six-membered rings. The formation of the rings is aided by the hexagonal periodic cell, with chains of four hydrogen bonds separating a molecule from its periodic image. The upper layer of molecules almost directly overlies the positions of the lower layer of molecules, resulting in a number of vertical four- and five-membered rings of molecules.

For the duration of the MD run, the system maintains this approximate structure, and therefore the energy of the system is fairly stable throughout. The energy can also be compared with that for a system where the hydrazine is not adsorbed at the surface. In Figure 8, the energy profile during the dynamics for the adsorbed hydrazine is generally more negative than that of the system with the free solvated hydrazine, indicating that adsorbed hydrazine is a more stable system.

In the MD simulation with the hydrazine not adsorbed on the surface but freely moving within the water, we observe more diffusion of the molecules, and optimization of various snapshots results in a number of different configurations.

Although there is no dissociation of the hydrazine molecule into two $-NH_2$ fragments, toward the end of the simulation proton exchange occurs between the species, as water donates a proton to the hydrazine molecule. The optimized structure after proton exchange is shown in Figure 7b. Hydrazine is a weak base with a pK_a of 8.10.[50] As the bare metal surface acts as a Lewis acid, it is likely that under these conditions some proportion of the protonated form would be observed. After proton exchange, the

dx.doi.org/10.1021/cm103164w |*Chem. Mater.* 2011, 23, 2718–2728

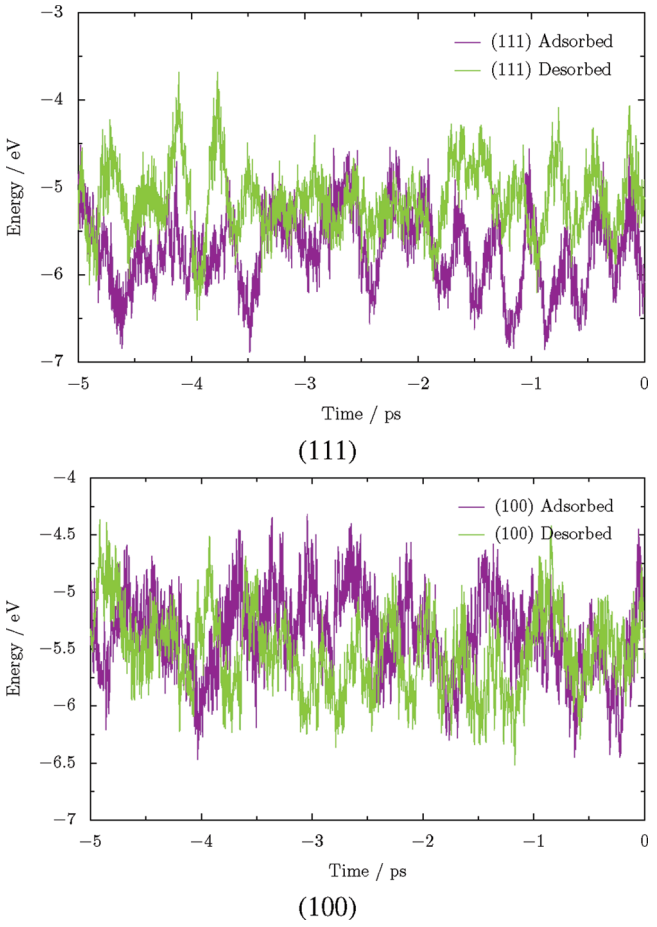

Figure 8. Energy profiles over time of adsorbed hydrazine on different copper surfaces during molecular dynamics. Profiles with the molecule adsorbed and desorbed are given for the final 5 ps of each simulation. The energy is shown as the difference from the isolated constituent molecules of the system.

hydrazine is effectively $NH_2NH_3^+$ and retains this structure until the end of the simulation. The corresponding OH^- formed in the process accepts four hydrogen bonds to its oxygen atom, compared to two for the majority of the water molecules in the structure. Energetically, this proton exchange does not seem to have a large effect on the overall stability of the structure; the most stable of these optimized structures are again determined by the extensive network of hydrogen bonding—the geometry in Figure 7c, for example, is more stable and no proton exchange has occurred. Although the OH^- is involved in one more hydrogen bond overall than a typical water molecule in the structure, the energy benefit is offset by the disruption of the regular hexagonal hydrogen-bonding network of the water molecules. This is compounded by the NH_3 end of the protonated hydrazine, which causes all three interacting water molecules to face away from the hydrazine, reducing the flexibility in forming networks of hydrogen bonds. In comparison, the more stable structures such as that in Figure 7c reveal layered ring structures, including molecules from the periodic images, with much closer registry between the upper and lower layers. In these structures, in contrast to the case where the hydrazine is bonded to the surface, a number of water molecules interact directly with the surface via their oxygen atoms. Whereas the isolated water molecules, described earlier in this work, lie flat on the surface, in this case they face upward to form hydrogen bonds.

Table 4. Configurational Binding Energy for Hydrazine Adsorbed with Water on Different Surfaces[a]

	(111) surface	(100) surface
adsorbed/eV	−5.72 (±0.40)	−5.37 (±0.35)
desorbed/eV	−5.15 (±0.38)	−5.53 (±0.35)
E_{ads}/eV	−0.57	0.16

[a] Values are calculated as the average over the final 5 ps of the dynamics simulation compared to the sum of the isolated constituent molecules and are listed with their standard deviations.

The torsional angle of the protonated hydrazine has only staggered or eclipsed states, and the molecule prefers to stagger the hydrogen atoms. The torsional angle for the unprotonated molecule stays close to the gauche conformer for the majority of the time, only rarely getting close to trans or eclipsed torsional angles, and the geometries with the molecule as the trans conformer do not show a significant energy difference from the geometries involving gauche conformers.

The individual snapshots relaxed to their local ground states tend to show more stable structures where the hydrazine is bridging the surface atoms. Averages of the energy of adsorption taken over a significant portion of the simulation, listed in Table 4, show that to adsorb the hydrazine on the surface from the solution would be a thermodynamically favorable process as the difference in energies is exothermic, albeit with a large error. The magnitude of this energy difference is also greater than the energies obtained from either the gas-phase adsorption or the competitive adsorption models.

(100) Surface. In gas-phase adsorption on the (100) surface, the hydrazine slightly favors a bridging configuration. In the initial configuration for the MD run, the molecule is adsorbed in a nonbridging geometry, but after about 4 ps the second nitrogen atom adsorbs to the neighboring surface copper atom. The molecule then stays in the bridging geometry for the rest of the simulation, oscillating between the two gauche torsional conformers and passing through the eclipsed conformation as it switches. At the stage when the molecule first makes the bridging configuration, the energy profile of the simulation descends to an energy minimum, after which the energy remains fairly stable for the remainder of the simulation. The optimized geometries of the bridging structures again provide the most stable configurations. In contrast with the (111) surface, the hydrazine in these structures is closer to the preferred gauche conformer.

The most stable structure from the snapshots for adsorption on the (100) surface is shown in Figure 9a, with Figure 9b showing the structure prior to bridge formation. Again, there is a very clear network of hydrogen bonds present and the hydrazine molecule is hydrogen-bonded to four different water molecules. The overall distribution of the water is, however, less regular than the layered series of ring structures that are formed on the (111) surface. In some of the optimized structures, voids appear as the system attempts to increase the hydrogen bonding in small clusters and cages of rings of hydrogen-bonded water. These structures are consequently less stable than the equivalent structures with hydrazine adsorbed on the (111) surface. The number density of water on the (100) surface is only 13% lower than on the (111) surface (0.20 compared to 0.23 $Å^{-2}$).

dx.doi.org/10.1021/cm103164w |*Chem. Mater.* 2011, 23, 2718–2728

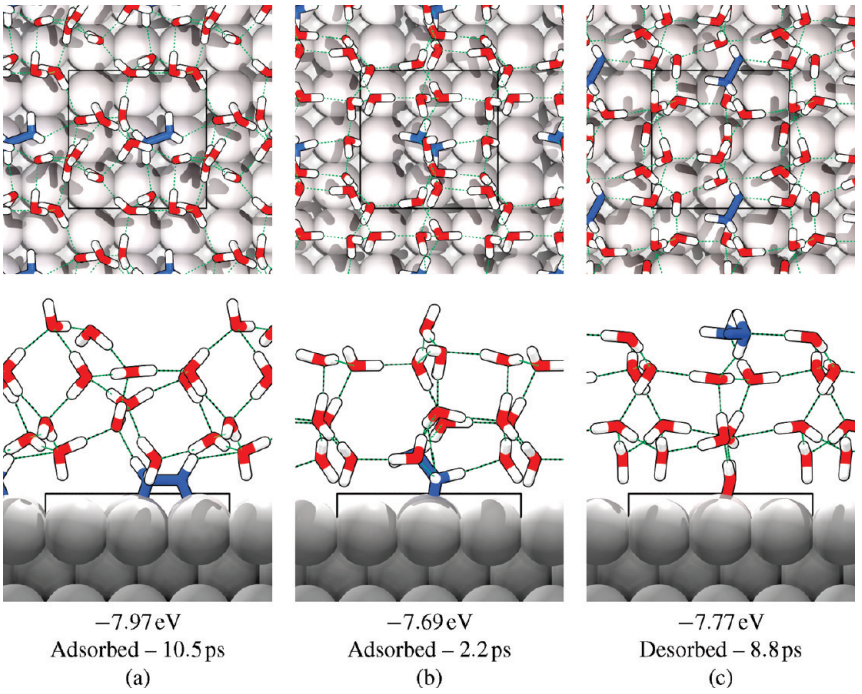

Figure 9. Optimized snapshots at the indicated times after equilibration, showing cooperative adsorption of hydrazine and water on the (100) surface (N = blue, O = red, H = white). Energies are the adsorption energy for the ground-state optimized structure from the gas phase per simulation cell.

The dynamics were also run with the hydrazine not adsorbed on the surface. Water replaces hydrazine at the surface and forms Cu−O bonds. The free hydrazine remains almost exclusively as the gauche conformer for the duration of the simulation. Upon optimization of the snapshot structures, the resulting geometries form six-membered rings both parallel and perpendicular to the surface. The most stable of these ground-state structures is shown in Figure 9c. The hydrazine is located at the interface with the vacuum, which excludes some of its hydrogen atoms from hydrogen bonding, although the molecule retains all the N···H−O_{water} hydrogen bonds. While the hexagonal symmetry of the (111) surface cell matched the symmetry of the ring structures, on the (100) surface the adsorbed molecules have become aligned more closely to the underlying square symmetry of the surface with a number of distinct rows and columns visible in the arrangement of the water molecules. This patterning could be due to the underlying symmetry of the surface atoms; however, it could equally be a result of the periodic constraints of the system. Further work would need to be carried out with larger systems to determine the effect of the underlying square lattice on the arrangement of water molecules.

Although the strongest adsorption is found with the hydrazine adsorbed on the surface, the energy difference between the two adsorption states of the molecule is much lower than on the (111) surface, as shown in the energy profile of the MD in Figure 8, which does not show any difference between the energy of the two states. Average values for the adsorption energies, given in Table 4, actually show a slight preference for desorption of the molecule (again with a significant statistical error), which is-the converse of the result on the (111) surface.

Summary. The structure and behavior of all the systems investigated are strongly determined by the hydrogen-bonding properties of the mixture. The models, when propagated with MD, provide structural and energetic information of the systems, which differ markedly from the gas phase adsorption studies.

The results of the cooperative hydrazine−water adsorption suggest a different ordering of adsorption strengths onto the surfaces from the gas-phase study. The adsorption is strongest on the (111) surface, and the molecule prefers to desorb from the (100) surface. The experimental results must therefore be rationalized differently. In the gas-phase study, hydrazine was assumed to poison growth on the surfaces that it binds to most strongly, leaving the (111) surfaces less occupied and therefore free to grow at a higher rate. However, experimentally the particle sizes increase with higher hydrazine concentrations, which does not agree with poisoned surface growth, or indeed the fact that hydrazine as the reducing agent promotes growth where it is located. Hydrazine adsorbed at a surface will reduce the metal ions at that surface to cause metal growth where it is adsorbed. The preferential adsorption at the (111) surfaces found in the present study will thus increase the growth rate there. With adsorption on the (100) surface disfavored, an increased hydrazine concentration will not have an impact on those surfaces. This differential adsorption behavior is in line with the change in experimental structures, which can be explained by preferential growth of the (111) faces. The effect of the greater hydrazine concentration in the reaction mixture will increase growth rate on all the surfaces, giving the larger particles, but particularly so on the (111) surfaces, leading to different particle morphologies. Of course, the model is still some way from accurately depicting the complete system for nanoparticle growth, and this conclusion is speculative and based only on the results presented here. Among the factors that would also need to be considered are the edge effects on the facets of a growing nanoparticle, which are not treated in the periodic system; the energy barriers for adsorption affecting the dynamics of the process; and the overall nanoparticle nucleation rate.

dx.doi.org/10.1021/cm103164w |*Chem. Mater.* 2011, 23, 2718–2728

Although the results have expanded significantly the previous work on this system and have led to much better insight, there is still room for improvement. The time scales simulated are still quite short; for example, taking the average energy over time has a standard deviation of 0.4 eV. As this is the same order of magnitude as the adsorption energies, longer simulations are needed to improve the statistical accuracy and reliability of the results, and with these large errors the conclusions based on the average energy cannot be firmly supported. The optimized snapshots do, however, already offer a more quantitative treatment of the configurations of the system that have been sampled. The methods of potential of mean force should be used with ab initio MD at solid−liquid interfaces for a rigorous treatment of the adsorption, but with an increased computational cost this is left for study in future work.[51−53]

In this study we began two trajectories on each surface; however, the impact of the initial configurations will not be realized without further simulation. While the hydrazine in the (100) surface system moved from a nonbridging to a bridging geometry, on the (111) surface system the bridging is imposed initially. Even if a nonbridging geometry is preferred, the system would be subject to energy barriers and time limitations that would prevent it from making the transition (although preliminary work on a third surface showed several transitions between bridging and nonbridging configurations). Furthermore, the initial configuration of the water and its fluctuations could have a larger effect on the energy than adsorption of the hydrazine. The size of the system is also important. Even though we have removed the interaction of a molecule with its periodic image, the periodic cell and its symmetry still have an influence on the geometry of the bonding. Increasing the cell size further could improve this but at an increased computational cost. It would also be necessary to increase the number of water molecules in the system, to ensure that complete coverage of the surface and solvation of the hydrazine is always achieved.

Finally, the DFT method accurately describes most of the system, except for the dispersive interactions. Although the magnitude of these forces will be relatively small, they are less rigidly structure-forming than hydrogen bonds and should be implemented to give the most complete description of the system.[54] Unfortunately, all of these improvements carry a significant computational cost. Even the systems modeled here required long calculations on massively parallel national high-performance computing facilities, making bigger systems and more accurate methods at present prohibitive. At the other end of the scale, deriving an empirical description of the system with interatomic potential methods would enable longer simulations of much larger systems, but current descriptions of the copper surface interactions are difficult to obtain and do not achieve the accuracy we need.

CONCLUSION

We have used DFT to model the behavior of hydrazine at copper (111) and (100) surfaces in the presence of water. Studying the competitive adsorption between the isolated hydrazine and water molecules is shown to be insufficient to describe the hydrazine−water−copper systems that are important in nanoparticle shape control.

The full system of hydrazine and water at the surfaces is shown to be strongly influenced by the network of hydrogen bonds that forms with the cooperative adsorption of the two species. In MD of the system, binding of the hydrazine to the surface is suggested to be a thermodynamically favorable process on the (111) surface but not on the (100) surface. These results of more realistic systems are substantially different from the previous gas-phase studies, showing the need to include explicitly solvent interactions when aqueous systems are studied. We can explain the experimental shapes of the copper nanoparticles by considering an excess of reducing agent at the (111) surfaces that promotes growth on those surfaces over the (100) surfaces.

AUTHOR INFORMATION

Corresponding Author

*E-mail t.daff@mail.cryst.bbk.ac.uk (T.D.D.), n.h.deleeuw@ucl.ac.uk (N.H.d.L.).

ACKNOWLEDGMENT

T.D.D. and N.H.d.L. acknowledge financial support from the Engineering and Physical Sciences Research Council (EPSRC) and thank Dr Isabelle Lisiecki for useful discussions. Via our membership in the United Kingdom's HPC Materials Chemistry Consortium, which is funded by EPSRC (EP/F067496 and EP/D504872), this work made use of the facilities of HECToR and HPCX.

REFERENCES

(1) Salzemann, C.; Lisiecki, I.; Brioude, A.; Urban, J.; Pileni, M. P. *J. Phys. Chem. B* **2004**, *108*, 13242–13248.
(2) Pileni, M. P. *Nanocrystals Forming Mesoscopic Structures*; Wiley−VCH: Berlin, 2005.
(3) Liu, W. T. *J. Biosci. Bioeng.* **2006**, *102*, 1–7.
(4) Scholes, G. D. *Adv. Funct. Mater.* **2008**, *18*, 1157–1172.
(5) Lee, K.; Kim, M.; Kim, H. *J. Mater. Chem.* **2010**, *20*, 3791–3798.
(6) Lisiecki, I.; Pileni, M. P. *J. Am. Chem. Soc.* **1993**, *115*, 3887–3896.
(7) Mohamed, M. B.; Wang, Z. L.; El-Sayed, M. A. *J. Phys. Chem. A* **1999**, *103*, 10255–10259.
(8) Jana, N. R.; Gearheart, L.; Murphy, C. J. *J. Phys. Chem. B* **2001**, *105*, 4065–4067.
(9) Wiley, B.; Herricks, T.; Sun, Y.; Xia, Y. *Nano Lett.* **2004**, *4*, 1733–1739.
(10) Grzelczak, M.; Perez-Juste, J.; Mulvaney, P.; Liz-Marzan, L. M. *Chem. Soc. Rev.* **2008**, *37*, 1783–1791.
(11) Xia, Y.; Xiong, Y.; Lim, B.; Skrabalak, S. E. *Angew. Chem.* **2009**, *48*, 60–103.
(12) Lisiecki, I.; Pileni, M. P. *Langmuir* **2003**, *19*, 9486–9489.
(13) Lisiecki, I. *J. Phys. Chem. B* **2005**, *109*, 12231–12244.
(14) Mott, D.; Galkowski, J.; Wang, L.; Luo, J.; Zhong, C. J. *Langmuir* **2007**, *23*, 5740–5745.
(15) Pileni, M. P. *Langmuir* **2001**, *17*, 7476–7486.
(16) Filankembo, A.; Giorgio, S.; Lisiecki, I.; Pileni, M. P. *J. Phys. Chem. B* **2003**, *107*, 7492–7500.
(17) Salzemann, C.; Lisiecki, L.; Urban, J.; Pileni, M. P. *Langmuir* **2004**, *20*, 11772–11777.
(18) Daff, T. D.; Saadoune, I.; Lisiecki, I.; de Leeuw, N. H. *Surf. Sci.* **2009**, *603*, 445–454.
(19) Daff, T. D.; Costa, D.; Lisiecki, I.; de Leeuw, N. H. *J. Phys. Chem. C* **2009**, *113*, 15714–15722.
(20) Cooper, T. G.; de Leeuw, N. H. *Langmuir* **2004**, *20*, 3984–3994.
(21) Zhou, Y.; Mazzolo, A.; Price, D. L.; Halley, J. W. *Int. J. Thermophys.* **1998**, *19*, 663–674.
(22) Izvekov, S.; Mazzolo, A.; VanOpdorp, K.; Voth, G. A. *J. Chem. Phys.* **2001**, *114*, 3248–3257.

(23) Schravendijk, P.; van der Vegt, N.; Delle Site, L.; Kremer, K. *ChemPhysChem* **2005**, *6*, 1866–1871.
(24) Ghiringhelli, L. M.; Hess, B.; van der Vegt, N. F. A.; Delle Site, L. *J. Am. Chem. Soc.* **2008**, *130*, 13460–13464.
(25) Calzolari, A.; Cicero, G.; Cavazzoni, C.; Di Felice, R.; Catellani, A.; Corni, S. *J. Am. Chem. Soc.* **2010**, *132*, 4790–4795.
(26) Kresse, G.; Hafner, J. *Phys. Rev. B* **1993**, *47*, 558.
(27) Kresse, G.; Hafner, J. *Phys. Rev. B* **1994**, *49*, 14251.
(28) Kresse, G.; Furthmüller, J. *Comput. Mater. Sci.* **1996**, *6*, 15.
(29) Kresse, G.; Furthmüller, J. *Phys. Rev. B* **1996**, *54*, 11169.
(30) Blöchl, P. E. *Phys. Rev. B* **1994**, *50*, 17953.
(31) Kresse, G.; Joubert, D. *Phys. Rev. B* **1999**, *59*, 1758.
(32) Perdew, J. P.; Chevary, J. A.; Vosko, S. H.; Jackson, K. A.; Pederson, M. R.; Singh, D. J.; Fiolhais, C. *Phys. Rev. B* **1992**, *46*, 6671.
(33) Perdew, J. P.; Chevary, J. A.; Vosko, S. H.; Jackson, K. A.; Pederson, M. R.; Singh, D. J.; Fiolhais, C. *Phys. Rev. B* **1993**, *48*, 4978.
(34) Matsumoto, M. *J. Chem. Phys.* **2007**, *126*, No. 054503.
(35) Fajin, J. L. C.; Illas, F.; Gomes, J. R. B. *J. Chem. Phys.* **2009**, *130*, No. 224702.
(36) Tang, Q.-L.; Chen, Z.-X. *Surf. Sci.* **2007**, *601*, 954–964.
(37) Sälli, E.; Jalkanen, J.-P.; Laasonen, K.; Halonen, L. *Mol. Phys.* **2007**, *105*, 1271–1282.
(38) Ranea, V. A.; Michaelides, A.; Ramírez, R.; Vergés, J. A.; de Andres, P. L.; King, D. A. *Phys. Rev. B* **2004**, *69*, No. 205411.
(39) Neves, R. S.; Motheo, A. J.; Fartaria, R. P. S.; Silva Fernandes, F. M. S. *J. Electroanal. Chem.* **2008**, *612*, 179–185.
(40) Nakamura, M.; Ito, M. *Chem. Phys. Lett.* **2004**, *384*, 256–261.
(41) Hodgson, A.; Haq, S. *Surf. Sci. Rep.* **2009**, *64*, 381–451.
(42) Asthagiri, D.; Pratt, L. R.; Kress, J. D. *Phys. Rev. E* **2003**, *68*, No. 041505.
(43) Collin, R. L.; Lipscomb, W. N. *Acta Crystallogr.* **1951**, *4*, 10–14.
(44) Kamishina, Y. *J. Magn. Reson.* **1975**, *20*, 388–393.
(45) Kristyán, S.; Pulay, P. *Chem. Phys. Lett.* **1994**, *229*, 175–180.
(46) Tsuzuki, S.; Luthi, H. P. *J. Chem. Phys.* **2001**, *114*, 3949–3957.
(47) Steiner, T.; Desiraju, G. R. *Chem. Commun. (Cambridge, U.K.)* **1998**, 891–892.
(48) Giordano, D. *J. Chem. Eng. Data* **2001**, *46*, 486–505.
(49) Liminga, R.; Olovsson, I. *Acta Crystallogr.* **1964**, *17*, 1523–1528.
(50) Hall, H. K. *J. Am. Chem. Soc.* **1957**, *79*, 5441–5444.
(51) Nair, N. N.; Schreiner, E.; Marx, D. *J. Am. Chem. Soc.* **2008**, *130*, 14148–14160.
(52) Cicero, G.; Grossman, J. C.; Schwegler, E.; Gygi, F.; Galli, G. *J. Am. Chem. Soc.* **2008**, *130*, 1871–1878.
(53) Leung, K.; Nielsen, I. M. B.; Criscenti, L. J. *J. Am. Chem. Soc.* **2009**, *131*, 18358–18365.
(54) Williams, R. W.; Malhotra, D. *Chem. Phys.* **2006**, *327*, 54–62.